The Research of Medical Science Review
ISSN: 3007-1208 & 3007-1216 Volume 3, Issue 10, 2025

EFFICIENT PHOTOCATALYTIC DEGRADATION OF REACTIVE RED 195 DYE BY FE–NI BIMETALLIC NANOPARTICLES SUPPORTED ON CROSS-LINKED CHITOSAN

Abid Hussain[1], Mohammed Jawwad Saif [*2]

[1,*2]*Department of Applied Chemistry, Government College University Faisalabad, Punjab, Pakistan,*

[*2]jawwadsaif@gcuf.edu.pk

DOI: https://doi.org/10.5281/zenodo.17431092

Keywords
Iron-Nickel bimetallic nanoparticles, cross-linked chitosan, dye removal, adsorption, wastewater treatment, nanocomposite.

Article History
Received: 27 August 2025
Accepted: 09 October 2025
Published: 24 October 2025

Copyright @Author
Corresponding Author: *
Mohammed Jawwad Saif

Abstract
Iron-nickel (Fe-Ni) bimetallic nanoparticles have gained significant attention due to their unique catalytic and adsorption properties. In this study, Fe-Ni bimetallic nanoparticles were synthesized and adsorbed onto cross-linked chitosan to create a novel nanocomposite for the removal of dye from aqueous solutions. The nanocomposite was characterized using XRD, SEM, FTIR analysis. The adsorption efficiency of the nanocomposite was evaluated for the removal of reactive red 195 (RR) dye under varying conditions of pH, contact time, and initial dye concentration. These cross-linked chitosan iron/nickel bimetallic nanoparticles showed high photocatalytic pastime underneath visible light irradiation at pH five. Finally, it becomes concluded that the cross-linked chitosan iron / nickel bimetallic nanoparticles proved to be one of the quality nanomaterials for the degradation of the aforementioned dye. This study highlights the potential of Fe-Ni/cross-linked chitosan nanocomposites as an efficient and eco-friendly adsorbent for dye removal from wastewater.

INTRODUCTION

Water pollution is one of the most pressing environmental challenges of the 21st century, with industrial effluents being a major contributor [1]. Among these effluents, synthetic dyes are particularly problematic due to their widespread use in industries such as textiles, paper, plastics, and cosmetics [2-4]. These dyes are not only aesthetically displeasing but also highly toxic, non-biodegradable, and resistant to conventional water treatment methods [5,6]. When discharged into water bodies, they can disrupt aquatic ecosystems, reduce sunlight penetration, and pose serious health risks to humans, including carcinogenic and mutagenic effect [70-10]. Methylene blue (MB) and Congo red (CR), for example, are colors that are often used and have been extensively studied for their environmental impact [11].

Traditional methods for dye removal, such as coagulation, flocculation, membrane filtration, and chemical oxidation, have several limitations [12-17]. These include high operational costs, low efficiency, and the generation of secondary pollutants [18-22]. Adsorption, on the other hand, has become a hopeful option because it is easy to use and doesn't cost much. and high efficiency [23-26]. Among the

various adsorbents, chitosan a natural biopolymer made from chitin has gotten a lot of attention because of its unique properties, such as Good biocompatibility, ease of biodegradation, and the availability of reactive functional groups (such as amino group and hydroxyl groups) that facilitate pollutant binding [27-31]. It is due to the chemical structure of chitosan, that emphasizes the presence of reactive amino groups that play a crucial role in adsorption processes [32,33].

However, the mechanical strength and adsorption capacity of chitosan can be further enhanced through chemical modification and the incorporation of nanoparticles [34,35]. Bimetallic nanoparticles, particularly those composed of iron and nickel (Fe-Ni), have shown great potential in environmental applications due to their synergistic properties [36]. Iron provides strong reducing capabilities and magnetic properties, while nickel enhances catalytic activity and stability [37,38]. When combined, these metals exhibit superior performance in pollutant degradation and adsorption compared to their monometallic counterparts [39,40].

Moreover, the adsorption of Fe-Ni nanoparticles onto a chitosan matrix can create a nanocomposite with enhanced surface area, porosity, and mechanical stability, making it an ideal candidate for wastewater treatment [41]. Cross-linking of chitosan is a crucial step in improving its chemical stability and mechanical strength [42]. Glutaraldehyde is commonly used as a cross-linking agent due to its ability to form stable covalent bonds with the amino groups of chitosan [43,44]. The process strengthens the chitosan structure and increases the number of sites available for nanoparticle and pollutant adsorption [45].

Despite the growing interest in bimetallic nanoparticles and chitosan-based adsorbents, there is limited research on the synthesis and application of Fe-Ni bimetallic nanoparticles adsorbed on cross-linked chitosan for dye removal [46-49]. This work seeks to fill the existing research gap by (1) synthesizing and characterizing Fe–Ni/chitosan nanocomposites and (2) assessing their adsorption performance toward Reactive Red 195 under different conditions. The outcomes of this study are expected to support the design of effective and environmentally sustainable adsorbents for wastewater purification, particularly in industrial applications.

Experimental

Reagents and Materials

Chitosan medium molecular weight, derived from shrimp shells, Iron (Fe^{+3}) acetate, Nickel (Ni^{+2}) acetate of analytical grade, Hydrazine Monohydrate reducing agent for nanoparticle synthesis, Methylene diphenyl isocyanate (MDI) cross-linking agent for chitosan, HCl (37%) used to dissolve chitosan, Reactive red 195 to check photocatalytic performance experiments, were bought from Sigma-Aldrich and utilized without additional purification.

Synthesis Fe/Ni BMNPs

For the synthesis of Fe–Ni BMNPs, 100 mL of distilled water was added to each of four separate 250 mL conical flasks. Then added the following amounts of salts of iron and nickel in the table given below separately. Then mixed all the solutions with constant stirring. After this added 5 ml of hydrazine monohydrate in all flasks dropwise and stayed overnight. Precipitates were formed and filtered. Then washed with distilled water several time and dried.

Table 1. Scheme of synthesized bimetallic composites

Sr. No.	Iron acetate	Nickel acetate	DI Water + Hydrazine Monohydrate
Flask#1	0.6 g	2.4g	100 ml + 5ml of Hydrazine
Flask #2	1.2 g	1.8 g	100 ml + 5ml of Hydrazine
Flask#3	1.8 g	1.2 g	100 ml + 5ml of Hydrazine
Flask#4	2.4 g	0.6 g	100 ml + 5ml of Hydrazine



Fig 1. Synthesis of Fe/Ni BMNPs

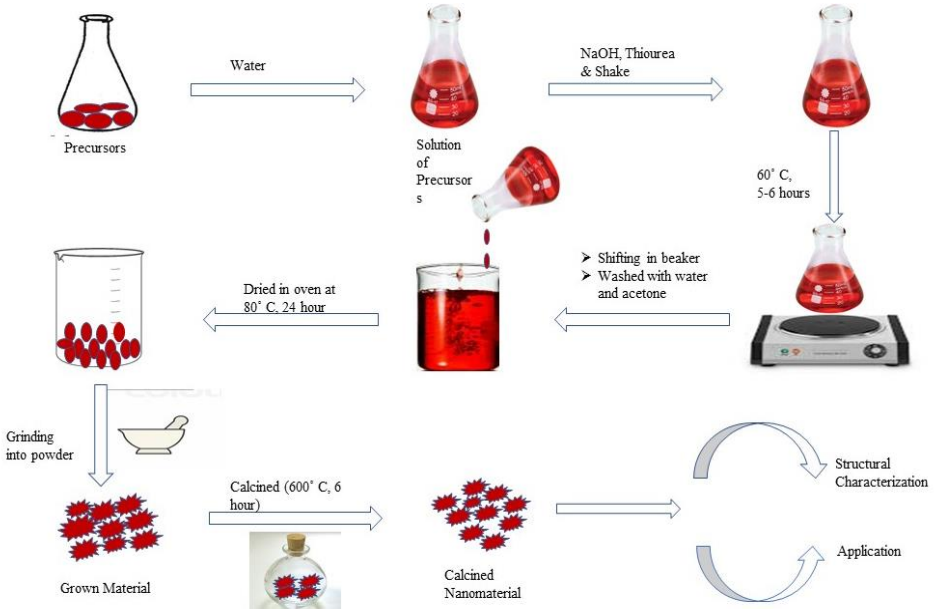


Fig 2. Flow sheet diagram for the synthesis of Samples [48]

Preparation Chitosan Solution

3% Chitosn solution was prepared in distilled water. For this purpose, dissolved 3 g Chitosan in 100 cm^3 of distilled water containing 5 ml of Hydrochloric acid (37%) solution to form Chitosan solution. This solution stirred at 600 rpm and 50 to 60 °C temperatures for 5 hours until Chitosan dissolved completely. It became transparent solution with light yellowish color and stayed overnight.

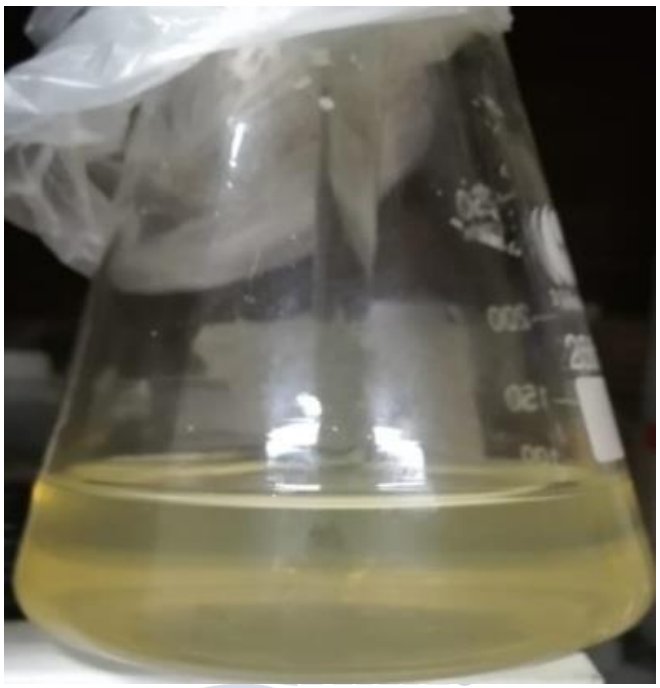


Fig 3. Yellowish colored solution of Chitosan

Institute for Excellence in Education & Research

Cross linking by MDI

Took 2 mL of above chitosan solution in 100 mL beaker. 2 mL MDI was added in this solution by drop wise at 50 oC and 1000 rpm for 1 hour. Then took it to universal sonication cleaner for 60 minutes. The solution became clear and stayed overnight.

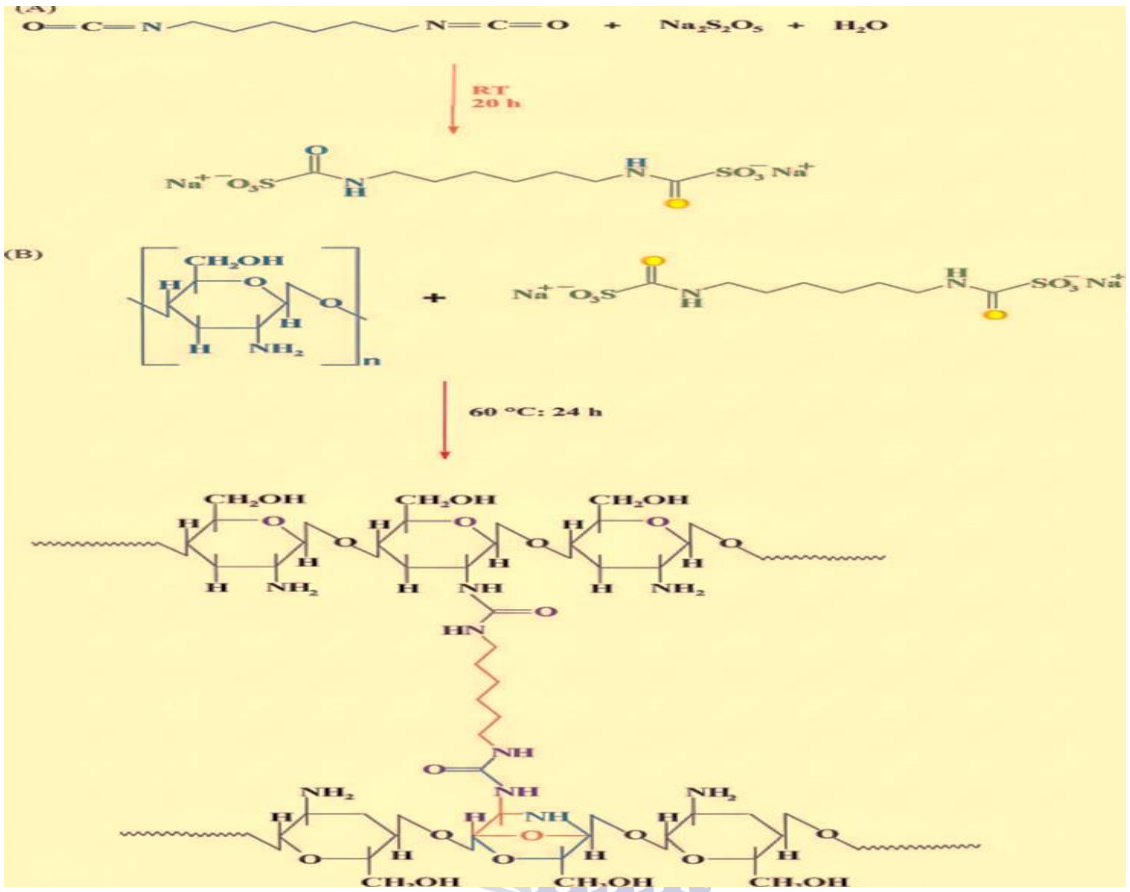


Fig 4. Solid-state mechanism of chitosan cross-linking using a water-soluble blocked diisocyanate [49].

Institute for Excellence in Education & Research

Synthesis of CSS Fe-Ni Beads

2 mL Chitosan solution took into 250 mL beaker. Drop wise 3 % 2 mL of Fe/Ni acetate salts of bimetallic solution (with composition 0.6g, 1.2g, 1.8g and 2.4g of Fe acetate and 2.4 g, 1.8g, 1.2g and 0.6g of Nickel acetate separately) were added into 2 mL Chitosan solution with constant stirrer at 800 rpm in 60 minutes. Then 2 mL MDI was added in this solution by drop wise at 40 °C and 1000 rpm for 1 hour. Then it took universal sonication cleaner for 60 minutes. The solution became clear and stayed overnight and slurry was formed. Then added 2 ml of hydrazine monohydrate dropwise in the slurry prepared for the reduction and stayed overnight. Then added drop wise 1% NaOH solution in above solution until pH came to 11. Precipitate formed and filtered the solution and washed the ppt with distilled water several time.



Fig 5. Images of All the Prepared Samples (CCS Fe-Ni)

Photocatalytic Degradation of RR 195 Dye

The photocatalytic performance of Fe-Ni bimetallic nano particles and their adsorbed composites on CCS was determined by photodegrading reactive-red 195 dye in aqueous solution under the UV light irradiation by filament. The general mechanism is explained in following figure 6.

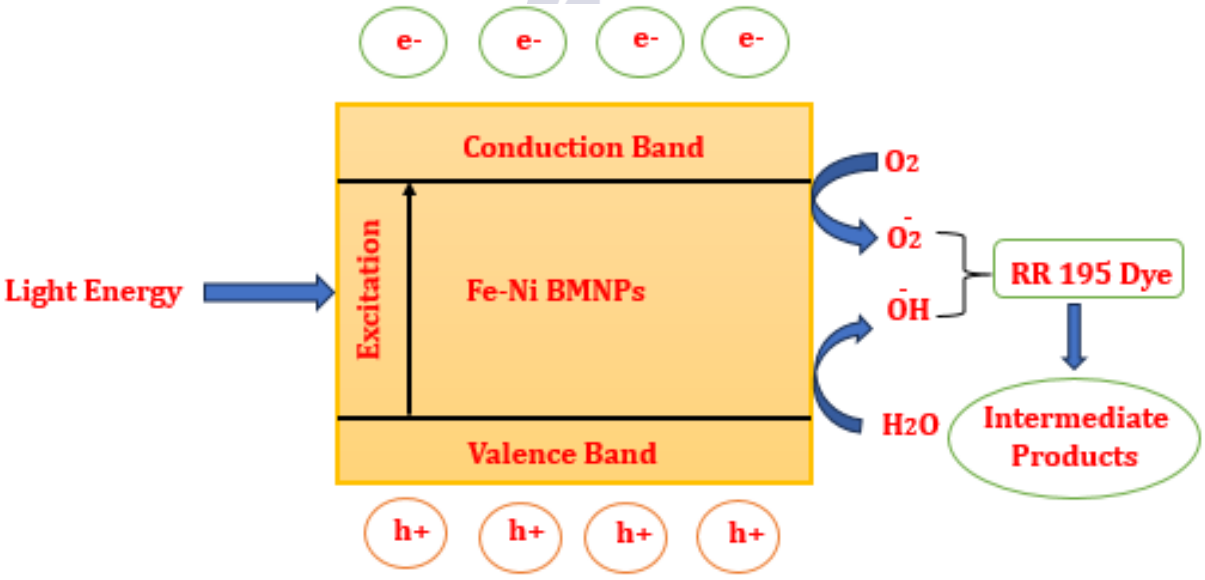


Fig 6. Scheme of the RR 195 removal from the aqueous phase by CCS-Fe Ni

The photocatalytic activity of the prepared composite was evaluated using a homemade setup. A 500 W xenon arc lamp was used to simulate sunlight. A dye solution was prepared by dissolving Reactive Red 195 in 1 L of deionized water. From this solution, 100 mL was transferred into separate glass tubes, and 0.01 g of each photocatalyst was added. The tubes were placed in the photocatalytic test box in the dark to achieve adsorption–desorption equilibrium by stirring for 1 hour. After this period, the dye–photocatalyst suspensions were continuously stirred under simulated sunlight irradiation (as illustrated in Fig. 7a and 7b).

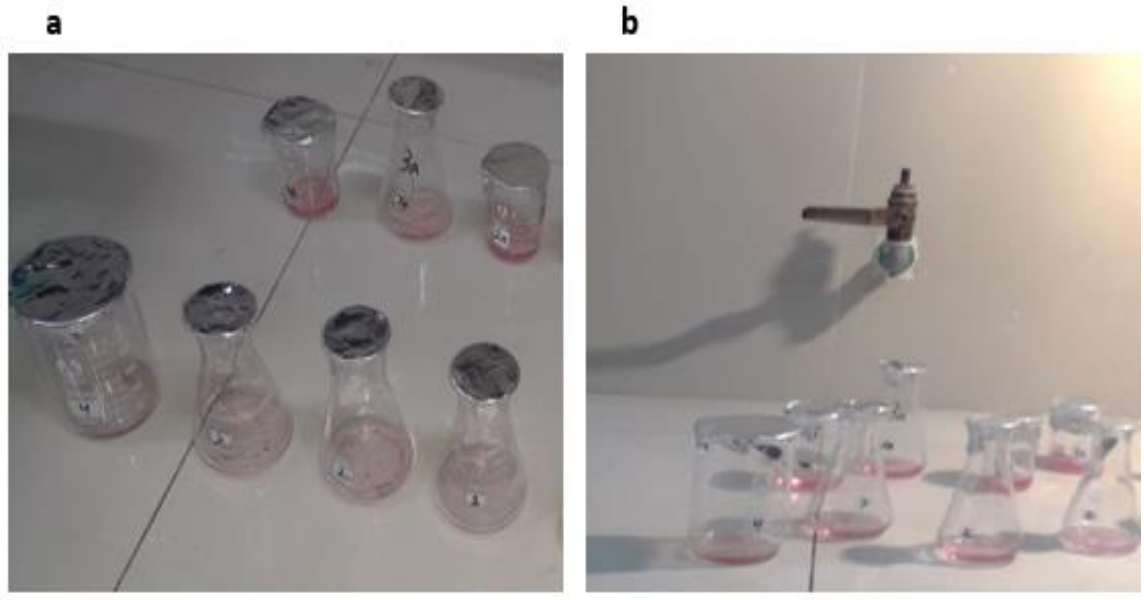


Fig 7. (a) Freshly prepared samples of RR 195 solution (b) during irradiation of these samples

The photocatalyst showed a diverse photocatalytic activity as shown in the fig 7, for degradation of reactive red 195 dye in the order of Fe-Ni nano composites composition 1 > Fe-Ni nano composites composition 4 > Fe-Ni nano composites composition 3 > Fe-Ni nano composites composition 2. The Fe–Ni nanocomposite of composition 1 exhibited the highest photodegradation rate after 60 minutes of irradiation, indicating that it was the most efficient photocatalyst among all those tested. Similarly for Fe-Ni nano composites adsorbed on CCS with composition 1 > Fe-Ni nano composites adsorbed on CCS with composition 4 > Fe-Ni nano composites adsorbed on CCS with composition 2> Fe-Ni nano composites adsorbed on CCS with composition 3.



Fig 8. Degraded samples of RR 195 solution with Fe-Ni NPs and with CCS Fe-Ni NPs

The highest photodegradation rate was observed for the Fe-Ni nano composites **sample 1 composition** after 60 minutes of irradiation, demonstrating that this photocatalyst outperformed all others. The result comparison of degradation of RR-195 dye in figure 9 a and c showed that Fe-Ni cross-linked chitosan sample played an important role in the photocatalytic performance with higher degradation efficiency than those of pure Fe-Ni nanocomposite in fig 9 b and d. Also, Due to high performance for degradation of RR 195 dye, sample 1 composition is further characterized to confirm the relative structural information.

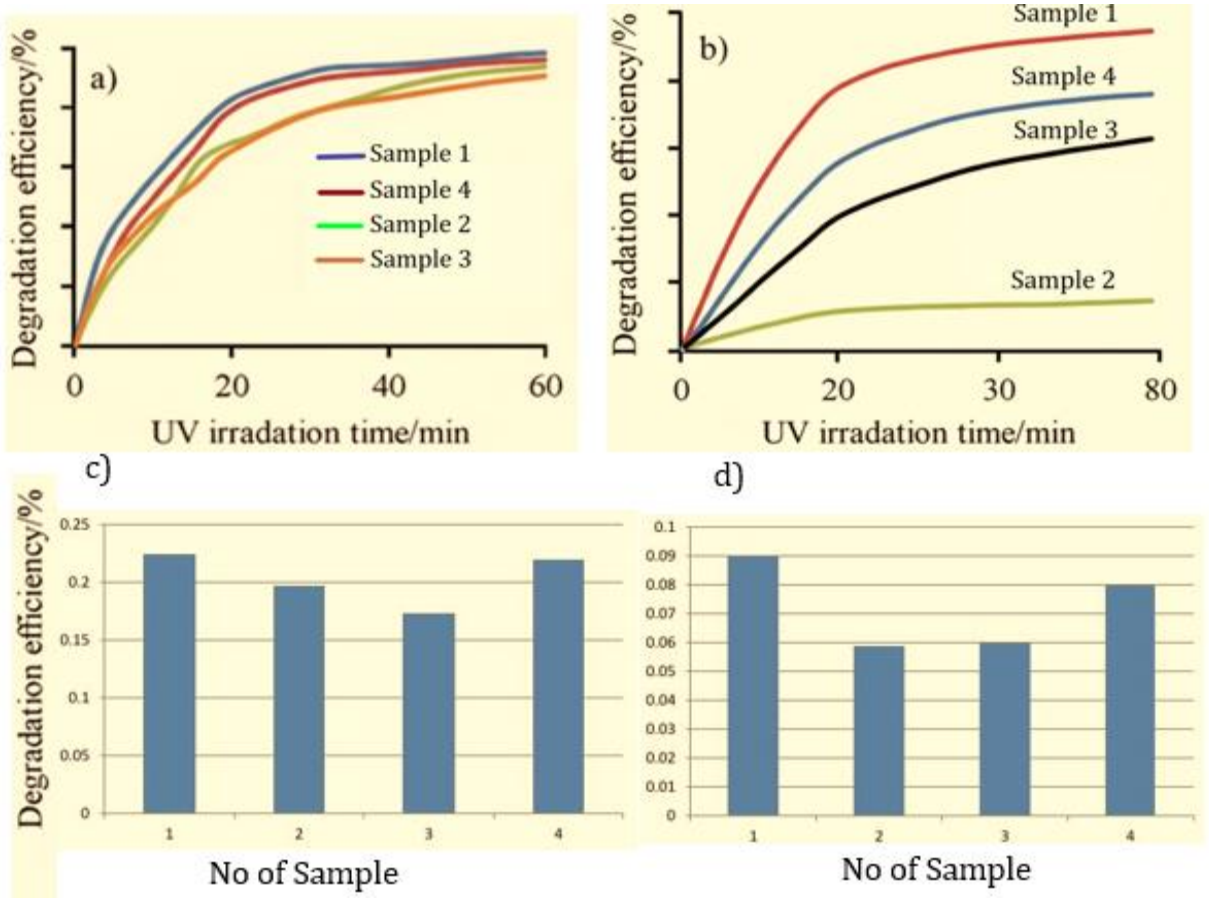


Fig 9. Study of photocatalytic performance on RR-195 dye concentration on degradation efficiency of novel catalysts prepared (a, c) Fe-Ni bimetallic nanoparticles adsorbed on cross-linked chitosan and (b, d) Fe-Ni bimetallic nanoparticles.

Instrumentation

The reagents and catalyst were accurately weighed using an OHAUS analytical balance. The photocatalytic degradation of dye solutions was monitored using a Bruker UV–Vis spectrophotometer. The textural and morphological features the materials were examined using a Bruker Field Emission Scanning Electron Microscope (FE-SEM) equipped with Energy-Dispersive X-ray Spectroscopy (EDX). The crystalline structure of the catalyst was determined using a Bruker D8 Advance X-ray Diffractometer (XRD) using Cu Kα radiation (λ = 1.5406 Å). The functional groups were detected on a Bruker Alpha II Fourier Transform Infrared (FTIR) spectrometer. Heating and stirring processes were performed using a Dragon Lab MS7-H550-Pro hotplate magnetic stirrer.

Results and Discussion

XRD Analysis

To establish the bimetallic nature and cross-linked samples of produced Fe-Ni NPs and CCS Fe-Ni NPs, XRD spectra were measured and reported in Fig 10 below. The background or support material, cross-linked chitosan, contributes a characteristic signal that typically dominates the low-angle region, [Broad Hump (Amorphous Phase)] The most defining feature of chitosan is often a broad, low-intensity peak or hump centered around 2θ≈20. This feature confirms the predominantly amorphous or semi-crystalline nature of the polymer, which is typical for polysaccharides [50-53]. (Effect of Cross-Linking) The original, non-cross-linked chitosan had sharper peaks (e.g., near 10 and 20 due to some crystallinity), the process of cross-linking was done by using MDI that disrupts the polymer's regular chain packing. This destruction of the ordered structure leads to the broadening (as shown in fig 10) and weakening of the chitosan peaks, confirming the successful formation of the cross-linked, more amorphous support matrix.

The presence of the Fe-Ni bimetallic nanoparticles is confirmed by a set of distinct, sharper peaks superimposed on the broad chitosan background. The specific location (the 2θ angle) and relative intensity of these peaks are used to identify the crystalline phase of the metal component, which could be an Fe-Ni alloy, a mixture of metal oxides (Fe_2O_3, NiO) [54-55]. For a typical Fe-Ni alloy (FCC structure), the main characteristic peaks would be expected at angles around 2θ≈40-45 corresponding to the (111), (200), and (220) crystallographic planes, respectively [56-59]. The peaks correspond to an Fe-Ni alloy phase, it confirms the successful formation of a bimetallic material where the iron and nickel atoms have alloyed into a single crystal structure, rather than simply existing as a mixture of separate iron and nickel phases [60]. The peaks from the Fe-Ni phase will be broader than those for a bulk (non-nano) material. This peak broadening is a direct measure of nanoparticles that have minuscule crystallite sizes, as described by the Debye-Scherrer equation. Broader peaks indicate smaller particle size [61,62]. The existence of crisp, well-defined band patterns at 2θ = 40 (111), 43 (200), and 44 (220) are steady with those found in the Joint Advisory group on Powder Diffraction Benchmarks (JCPDS) database, the signals corresponding to Fe and Ni in the Fe–Ni nanoparticles confirm the formation of bimetallic Fe–Ni NPs. [63-65].

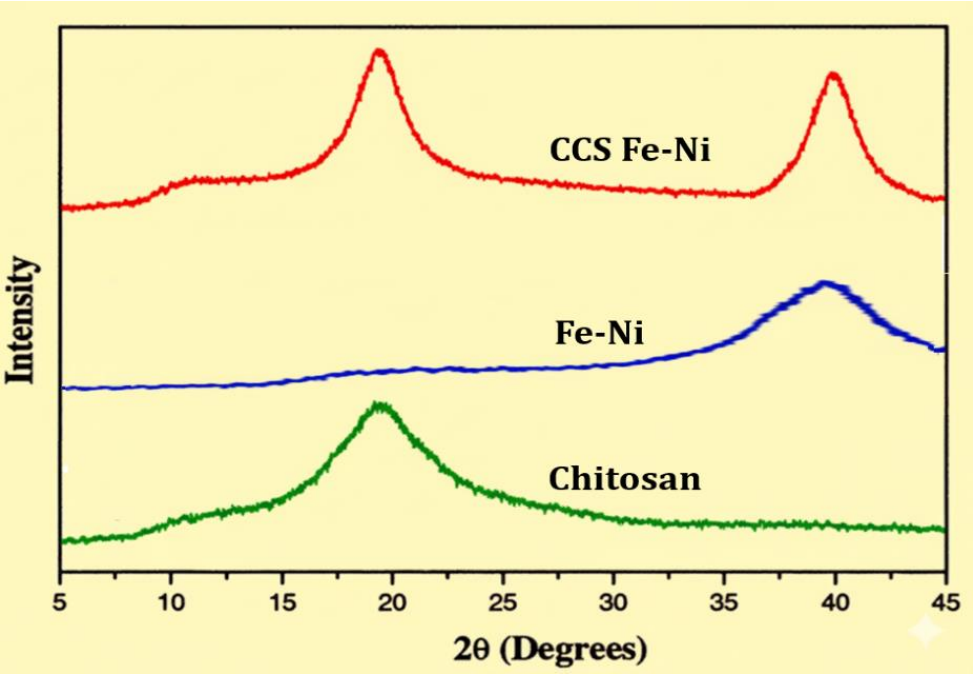


Fig 10. PXRD pattern of chitosan, Fe-Ni NPs and CSS Fe-Ni BMNPs

Overall, the PXRD pattern confirms (1) successful composite formation, evidenced by the amorphous peak of cross-linked chitosan and the sharp peaks of crystalline Fe-Ni nanoparticles [66], and (2) the structural state, where the broadened metal peaks indicate nanoscale dimensions, and the weak, broad polymer peak reflects the amorphous matrix, suitable for supporting and dispersing nanoparticles [67,68].

Interpretation of the Structural Parameters

The table 2 provides numerical values that support the qualitative observations from the patterns and demonstrate the structural changes in chitosan upon modification and/or cross-linking, primarily showing a potential initial change in structure (sample 0.0) followed by a substantial loss of crystalline order (peak broadening) when the cross-linker amount is increased (sample 0.2).

The structural parameters presented in the table, derived from Wide-Angle X-ray Diffraction (WAXD) patterns, quantitatively illustrate the changes in the crystalline structure of chitosan upon modification and/or cross-linking. The pure chitosan sample exhibits a principal crystalline reflection at 2θ≈20.4° (corresponding to the (110, 040) plane) with a FWHM of 2.67. The "0.0" sample shows a slight shift in the peak position to 19.9° and a notable decrease in fwhm to 1.60, suggesting that this initial modification (potentially a control treatment or a different precursor) results in a more ordered or crystalline structure compared to the original chitosan. However, when the cross-linking agent is introduced, as shown by the "0.2" sample, the most significant change is observed in the (110, 040) plane: the fwhm dramatically increases to 5.00. This substantial peak broadening is the key indicator of the cross-linking effect, signifying a disruption of the ordered crystalline structure and a reduction in the mean crystallite size due to the introduction of chemical bridges between the chitosan chains.

Table 2. Structural Characteristics Derived from WAXD Patterns

Sample	Plane	2(ø)	d(Å)	fwhm
Chitosan	(020)	10.8	8.37	2.47
	(110,040)	20.4	4.48	2.67
0.0	(020)	10.4	8.73	2.88
	(110,040)	19.9	4.58	1.60
	(101)	22.0	4.16	1.88
0.2	(110,040)	20.3	4.51	5.00

IIER
Institute for Excellence in Education & Research

"Here, 2θ shows the peak position, d is the spacing between crystal planes, and fwhm is the peak width at half its height"

FTIR Analysis

Based on the chemical composition of the materials, the Fourier-Transform Infrared (FTIR) spectrum of the pure Fe-Ni bimetallic nanoparticles (Figure 11) is appeared to be fundamentally different from the spectrum of the Cross-Linked Chitosan Supported Fe-Ni Bimetallic Nanoparticles (Figure 11), primarily due to the presence of the chitosan polymer matrix and its chemical interaction with the nanoparticles. The most significant difference that confirms the successful synthesis of the Cross-Linked Chitosan Supported Fe-Ni Bimetallic Nanoparticles (Figure 11) is the presence of the chitosan's characteristic organic peaks and the subsequent evidence of interaction with the metal nanoparticles [69,70].

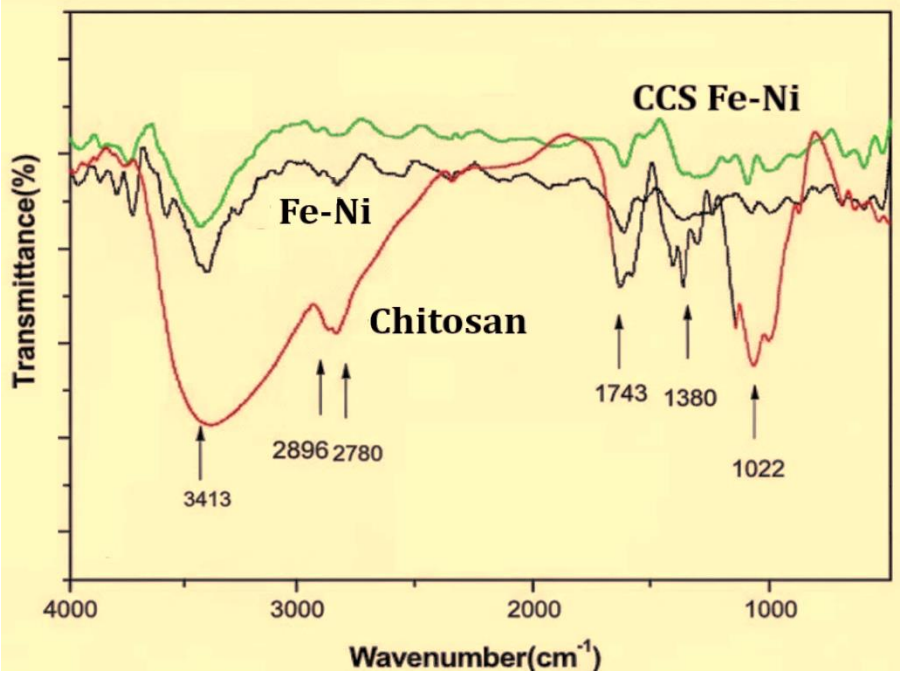


Fig. 11. FTIR Spectrum of chitosan, Fe-Ni NPs and CSS Fe-Ni BMNPs

Appearance of Chitosan Peaks: The above spectra exhibit the full suite of C-O, N-H, and C-H vibrational bands characteristic of the polymer that are completely absent in Figure 11, except for simple surface-adsorbed species [71].

Shifts in Chitosan Peaks (Evidence of Interaction/Chelation): The characteristic O–H and N–H stretching vibrations (around 3413 cm^{-1}) and the C=O or N–H bending vibrations (around 1650–1743 cm^{-1}) are shifted relative to pure chitosan, which forms part of the cross-linked matrix. These shifts result from interactions involving the functional groups of chitosan, particularly the amine (–NH_2) and hydroxyl (–OH) groups have participated in chelation or coordination with the Fe and Ni ions/nanoparticles, which is the mechanism of successful support and immobilization.

Presence of M-O Peaks: The spectra contain the characteristic low-wavenumber bands (400−700 cm−1) confirming the Fe-O and Ni-O vibrational modes, which indicates the presence of the bimetallic nanoparticles in both samples [72].

SEM / EDS Analysis

The SEM images (Fig 12 a, b and c) highlight the structural differences between unsupported and CCS Fe-Ni NPs. The unsupported nanoparticles appear as large, irregular clusters due to strong magnetic interactions and high surface energy, which cause severe agglomeration and poor dispersion. In contrast, the supported nanoparticles form more compact, rounded microstructures with a textured surface, where the metal particles are visibly anchored to the chitosan matrix. This polymeric support not only immobilizes the nanoparticles into defined shapes but also reduces random clumping, improves dispersion, and stabilizes the composite. Overall, the transition from chaotic aggregation to discrete, spheroidal structures confirms the successful synthesis of chitosan-supported Fe-Ni BMNPs with enhanced stability and surface characteristics.

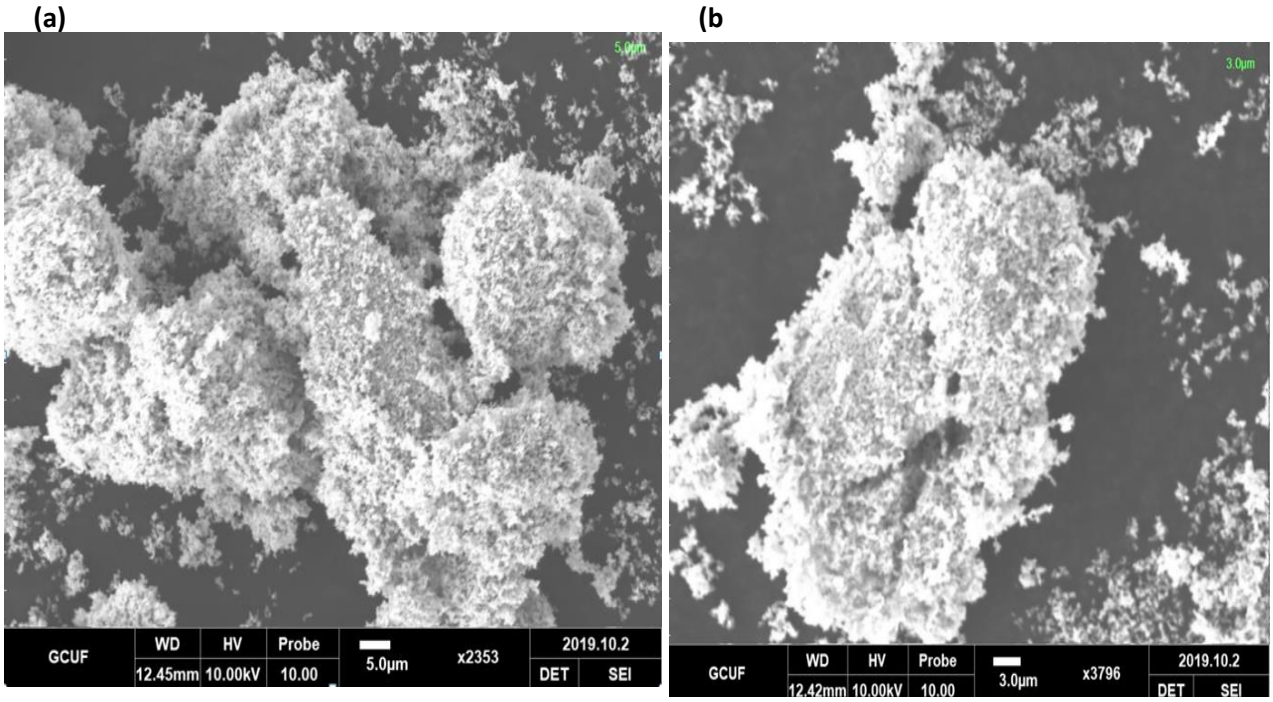


Fig 12. (a) SEM micrograph of Fe–Ni NPs (5.0 µm), and (b) SEM micrograph of CSS–Fe–Ni NPs (3.0 µm)

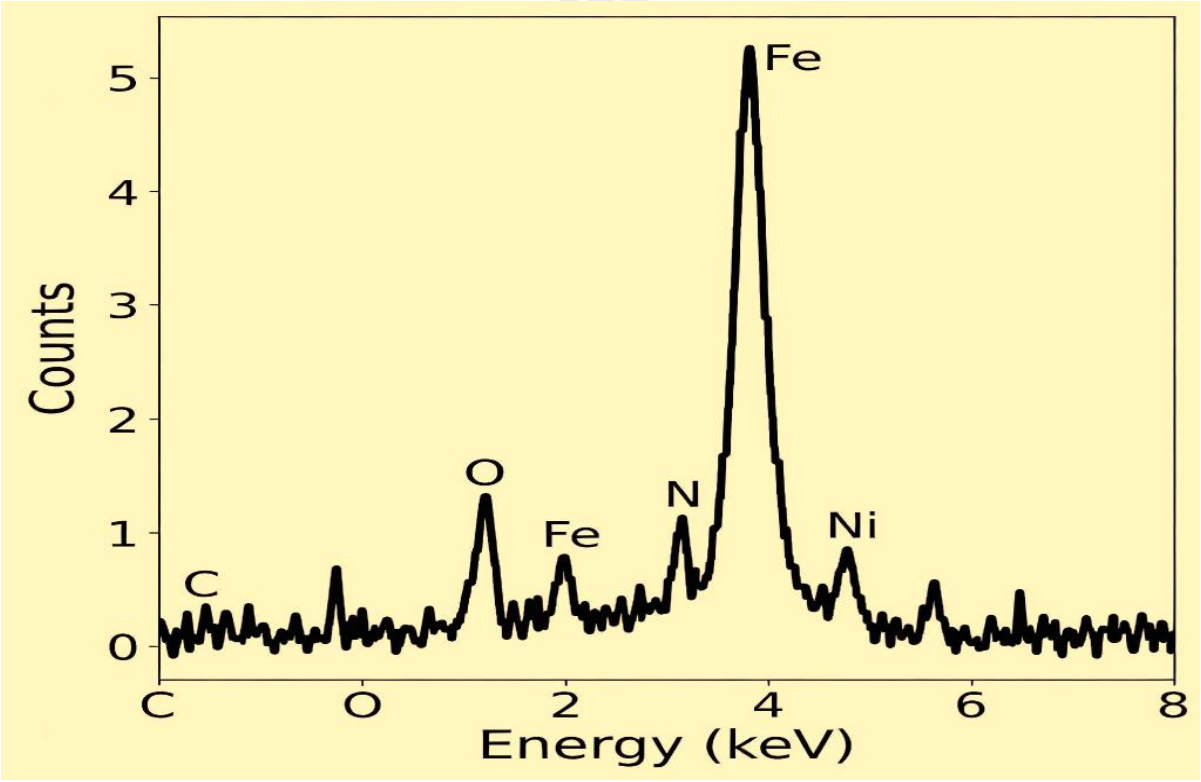


Fig 12. (c) Elemental mapping (EDS) of CSS Fe-Ni NPs

Conclusions

Iron/nickel bimetallic nanoparticles and cross-linked chitosan iron/nickel nanocomposites were successfully synthesized using the co-precipitation method at low temperature. XRD analysis confirmed their crystalline nature and indicated the absence of impurities. SEM/EDS images revealed that the bimetallic nanoparticles possessed a spherical morphology with uniform size, while in the cross-linked composite, the nanoparticles were encapsulated within the chitosan matrix with minor agglomeration, which could be reduced upon proper dispersion. FTIR spectra showed clear shifts in the characteristic peaks of chitosan, confirming the effective incorporation of iron/nickel bimetallic nanoparticles into the cross-linked polymer framework. Photocatalytic performance of both nanomaterials was examined for the degradation of Reactive Red 195 dye under controlled conditions. While the two samples of iron/nickel nanoparticles displayed strong catalytic efficiency however, the cross-linked chitosan iron/nickel nanocomposite exhibited significantly higher degradation performance, demonstrating its superior potential as a sustainable and efficient catalyst for dye removal applications.

Acknowledgments

The authors are thankful to the Department of Applied Chemistry, Government College University, Faisalabad, Punjab, Pakistan, for providing laboratory facilities and research advice. The authors also acknowledge the academics and staff for their invaluable support with experimental work and data processing.

Note: The authors disclose no competing financial interests.

REFERENCES

Arancibia-Miranda, N., Baltazar, S. E., García, A., Muñoz-Lira, D., Sepúlveda, P., Rubio, M. A., & et al. (2016). Nanoscale zero-valent iron supported by zeolite and montmorillonite: Template effect on the removal of lead ions from aqueous solution. *Journal of Hazardous Materials, 301*, 371–380.

Crane, R. A., & Sapsford, D. J. (2017). Selective formation of copper nanoparticles from acid mine drainage using nanoscale zerovalent iron particles. *Journal of Hazardous Materials, 347*, 252–265.

Dong, H., Guan, X., Wang, D., & Ma, J. (2011). Individual and combined influence of calcium and anions on simultaneous removal of chromate and arsenate by Fe(II) under suboxic conditions. *Separation and Purification Technology, 80*, 284–292.

Dong, H., Qi, H., Zeng, G., Lin, T., Chang, Z., Xie, Y., *et al.* (2016a). Chromate removal by surface-modified nanoscale zero-valent iron: Effect of different surface coatings and water chemistry. *Journal of Colloid and Interface Science, 471*, 7–13.

Dong, H., Xie, Y., Zeng, G., Lin, T., Jie, L., Qi, H., *et al.* (2016b). The dual effects of carboxymethyl cellulose on the colloidal stability and toxicity of nanoscale zero-valent iron. *Chemosphere, 144*, 1682–1689.

Dong, H., Zeng, Y., Zeng, G., Huang, D., Liang, J., Zhao, F., *et al.* (2016c). EDDS-assisted reduction of Cr(VI) by nanoscale zero-valent iron. *Separation and Purification Technology, 165*, 86–91.

Dong, H., Jiang, Z., Deng, J., Zhang, C., Cheng, Y., Hou, K., *et al.* (2017a). Physicochemical transformation of Fe/Ni bimetallic nanoparticles during aging in simulated groundwater and the consequent effect on contaminant removal. *Water Research*, 51–57.

Dong, H., Zeng, Y., Xie, Y., He, Q., Zhao, F., Wang, Y., *et al.* (2017b). Single and combined removal of Cr(VI) and Cd(II) by nanoscale zero-valent iron in the absence and presence of EDDS. *Water Science and Technology, 76*, 1261–1271.

Dong, H., Zhao, F., He, Q., Xie, Y., Zeng, Y., Zhang, L., *et al.* (2017c). Physicochemical transformation of carboxymethyl cellulose-coated zero-valent iron nanoparticles (nZVI) in simulated groundwater under anaerobic conditions. *Separation and Purification Technology, 175*, 376–383.

Feng, J., & Lim, T. T. (2005). Pathways and kinetics of carbon tetrachloride and chloroform reductions by nano-scale Fe and Fe/Ni particles: Comparison with commercial microscale Fe and Zn. *Chemosphere, 59*, 1267–1273.

Gao, Y., Wang, F., Wu, Y., Naidu, R., & Chen, Z. (2016). Comparison of degradation mechanisms of microcystin-LR using nanoscale zero-valent iron (nZVI) and bimetallic Fe/Ni and Fe/Pd nanoparticles. *Chemical Engineering Journal, 285*, 459–466.

Geng, B., Jin, Z., Li, T., & Qi, X. (2009a). Kinetics of hexavalent chromium removal from water by chitosan–Fe^0 nanoparticles. *Chemosphere, 75*, 825–830.

Geng, B., Jin, Z., Li, T., & Qi, X. (2009b). Preparation of chitosan-stabilized Fe^0 nanoparticles for removal of hexavalent chromium in water. *Science of the Total Environment, 407*, 4994–5000.

Gong, X., Huang, D., Liu, Y., Zeng, G., Wang, R., Wan, J., *et al.* (2017a). Stabilized nanoscale zero-valent iron mediated cadmium accumulation and oxidative damage of *Boehmeria nivea* (L.) Gaudich cultivated in cadmium contaminated sediments. *Environmental Science & Technology, 51*, 11308–11316.

Gong, Y., Gai, L., Tang, J., Fu, J., Wang, Q., & Zeng, E. Y. (2017b). Reduction of Cr(VI) in simulated groundwater by FeS-coated iron magnetic nanoparticles. *Science of the Total Environment, 595*, 743–751.

Horzum, N., Demir, M. M., Nairat, M., & Shahwan, T. (2013). Chitosan fiber-supported zero-valent iron nanoparticles as a novel sorbent for sequestration of inorganic arsenic. *RSC Advances, 3*, 7828–7836.

Hu, C. Y., Lo, S. L., Liou, Y. H., Hsu, Y. W., Shih, K., & Lin, C. J. (2010). Hexavalent chromium removal from near natural water by copper–iron bimetallic particles. *Water Research, 44*, 3101–3108.

Hu, X. J., Wang, J. S., Liu, Y. G., Li, X., Zeng, G. M., Bao, Z. L., *et al.* (2011). Adsorption of chromium (VI) by ethylenediamine-modified cross-linked magnetic chitosan resin: Isotherms, kinetics and thermodynamics. *Journal of Hazardous Materials, 185*, 306–314.

Huang, D. L., Chen, G. M., Zeng, G. M., Xu, P., Yan, M., Lai, C., *et al.* (2015). Synthesis and application of modified zero-valent iron nanoparticles for removal of hexavalent chromium from wastewater. *Water, Air, and Soil Pollution, 226*, 375.

Huang, D., Xue, W., Zeng, G., Wan, J., Chen, G., Huang, C., *et al.* (2016). Immobilization of Cd in river sediments by sodium alginate modified nanoscale zero-valent iron: Impact on enzyme activities and microbial community diversity. *Water Research, 106*, 15–25.

Kazemi, M. O., Jahanshahi, M., & Peyravi, M. (2018). Hexavalent chromium removal by multilayer membrane assisted by photocatalytic couple nanoparticle from both permeate and retentate. *Journal of Hazardous Materials, 344*, 12–22.

Kumar, M. A., Bae, S., Han, S., Chang, Y., & Lee, W. (2017). Reductive dechlorination of trichloroethylene by polyvinylpyrrolidone-stabilized nanoscale zerovalent iron particles with Ni. *Journal of Hazardous Materials, 340*, 399–407.

Kumarathilaka, P., Jayaweera, V., Wijesekara, H., Kottegoda, I. R. M., Rosa, S. R. D., & Vithanage, M. (2016). Insights into starch-coated nano zero-valent iron–graphene composite for Cr(VI) removal from aqueous medium. *Journal of Nanomaterials, 2016*, Article 7.

Kustov, L. M., Finashina, E. D., Shuvalova, E. V., Tkachenko, O. P., & Kirichenko, O. A. (2011). Pd–Fe nanoparticles stabilized by chitosan derivatives for perchloroethene dechlorination. *Environment International, 37*, 1044–1051.

Li, H., Ge, Y., & Zhang, X. (2016). High efficient removal of lead from aqueous solution by preparation of novel PPG-nZVI beads as sorbents. *Colloids and Surfaces A: Physicochemical and Engineering Aspects, 513*, 120–127.

Li, J., Zhang, X., Sun, Y., Liang, L., Pan, B. C., Zhang, W., *et al.* (2017a). Advances in sulfidation of zerovalent iron for water decontamination. *Environmental Science & Technology, 248*, 173–182.

Li, Y., Li, X., Han, D., Huang, W., & Yang, C. (2017b). New insights into the role of Ni loading on the surface structure and reactivity of nZVI toward tetrabromo- and tetrachlorobisphenol A. *Chemical Engineering Journal, 311*, 173–182.

Liang, D. W., Yang, Y. H., Xu, W. W., Peng, S. K., Lu, S. F., & Xiang, Y. (2014). Nonionic surfactant greatly enhances the reductive debromination of polybrominated diphenyl ethers by nanoscale zero-valent iron: Mechanism and kinetics. *Journal of Hazardous Materials, 278*, 592–596.

Ling, L., Huang, X. Y., Li, M., & Zhang, W. X. (2017). Mapping the reactions in a single zero valent iron nanoparticle. *Environmental Science & Technology, 51*, 14293–14300.

Liu, T., Yang, X., Wang, Z. L., & Yan, X. (2013). Enhanced chitosan beads-supported Fe(0) nanoparticles for removal of heavy metals from electroplating wastewater in permeable reactive barriers. *Water Research, 47*, 6691–6699.

Liu, F., Shan, C., Zhang, X., Zhang, Y., Zhang, W., & Pan, B. (2017). Enhanced removal of EDTA-chelated Cu(II) by polymeric anion-exchanger supported nanoscale zero-valent iron. *Journal of Hazardous Materials, 321*, 290–298.

Lv, Y., Niu, Z., Chen, Y., & Hu, Y. (2017). Bacterial effects and interfacial inactivation mechanism of nZVI/Pd on *Pseudomonas putida* strain. *Water Research, 115*, 297–308.

Naim, M. M., El-Shafei, A. A., Elewa, M. M., & Moneer, A. A. (2016). Application of silver-, iron-, and chitosan-nanoparticles in wastewater treatment. *International Conference of European Desalination Society, Desalination for Environment: Clean Water and Energy*, 268–280.

Nakseedee, P., Tanboonchuy, V., Khemthong, P., Grisdanurak, N., & Liao, C.-H. (2017). Role of Cu on zero valent bimetallic Cu–Fe in arsenic removal with gas bubbling. *Environmental Progress & Sustainable Energy, 36*, 1449–1457.

Peng, Z., Xiong, C., Wei, W., Tan, F., Yang, X., Wang, X., *et al.* (2017). Facile modification of nanoscale zero-valent iron with high stability for Cr(VI) remediation. *Science of the Total Environment, 596–597*, 266–273.

Qian, L., Zhang, W., Yan, J., Han, L., Chen, Y., Ouyang, D., *et al.* (2017). Nanoscale zero-valent iron supported by biochars produced at different temperatures: Synthesis mechanism and effect on Cr(VI) removal. *Environmental Pollution, 223*, 153–160.

Qu, G., Kou, L., Wang, T., Liang, D., & Hu, S. (2017). Evaluation of activated carbon fiber supported nanoscale zero-valent iron for chromium (VI) removal from groundwater in a permeable reactive column. *Journal of Environmental Management, 201*, 378–387.

Shi, L.-N., Zhang, X., & Chen, Z.-L. (2011). Removal of chromium (VI) from wastewater using bentonite-supported nanoscale zero-valent iron. *Water Research, 45*, 886–892.

Soliemanzadeh, A., & Fekri, M. (2017). The application of green tea extract to prepare bentonite-supported nanoscale zero-valent iron and its performance on removal of Cr(VI): Effect of relative parameters and soil experiments. *Microporous and Mesoporous Materials, 239*, 60–69.

Stefaniuk, M., Oleszczuk, P., & Yong, S. O. (2016). Review on nano zerovalent iron (nZVI): From synthesis to environmental applications. *Chemical Engineering Journal, 287*, 618–632.

Tian, H., Liang, Y., Zhu, T., Zeng, X., & Sun, Y. (2018). Surfactant-enhanced PEG-4000-NZVI for remediating trichloroethylene-contaminated soil. *Chemosphere, 195*, 585–593.

Theron, J., Walker, J. A., & Cloete, T. E. (2008). Nanotechnology and water treatment: Applications and emerging opportunities. *Critical Reviews in Microbiology, 34*(1), 43–69.

Tian, H., Li, J., Mu, Z., Li, L., & Hao, Z. (2009). Effect of pH on DDT degradation in aqueous solution using bimetallic Ni/Fe nanoparticles. *Separation and Purification Technology, 66*(1), 84–89.

IEER Institute for Excellence in Education & Research

Tisa, F., Aziz, A., Raman, A. A. A., Mohd, W. M. A. W., & Wan, A. (2014). Applicability of fluidized bed reactor in recalcitrant compound degradation through advanced oxidation processes: A review. *Journal of Environmental Management, 146*, 260–275.

Vilardi, G., Di Palma, L., & Verdone, N. (2019a). A physical-based interpretation of mechanism and kinetics of Cr(VI) reduction in aqueous solution by zero-valent iron nanoparticles. *Chemosphere, 220*, 590–599.

Vilardi, G., Rodriguez-Rodriguez, J., Ochando-Pulido, J. M., Di Palma, L., & Verdone, N. (2019b). Fixed-bed reactor scale-up and modelling for Cr(VI) removal using nano iron-based coated biomass as packing material. *Chemical Engineering Journal, 361*, 990–998.

Wang, D., & Li, Y. (2011). Bimetallic nanocrystals: Liquid-phase synthesis and catalytic applications. *Advanced Materials, 23*, 1044–1060.

Wang, T., Lin, J., Chen, Z., Megharaj, M., & Naidu, R. (2014). Green synthesized iron nanoparticles by green tea and eucalyptus leaf extracts used for removal of nitrate in aqueous solution. *Journal of Cleaner Production, 83*, 413–419.

Wang, J., Liu, C., Hussain, I., Li, C., Li, J., Sun, X., Shen, J., Han, W., & Wang, L. (2016). Iron–copper bimetallic nanoparticles supported on hollow mesoporous silica spheres: The effect of Fe/Cu ratio on heterogeneous Fenton degradation of a dye. *RSC Advances, 6*, 54623–54635.

Weng, X., Lin, S., Zhong, Y., & Chen, Z. (2013). Chitosan-stabilized bimetallic Fe/Ni nanoparticles used to remove mixed contaminants—amoxicillin and Cd(II)—from aqueous solutions. *Chemical Engineering Journal, 229*, 27–34.

Weng, X., Sun, Q., Lin, S., Chen, Z., Megharaj, M., & Naidu, R. (2014). Enhancement of catalytic degradation of amoxicillin in aqueous solution using clay-supported bimetallic Fe/Ni nanoparticles. *Chemosphere, 103*, 80–85.

Xie, Y., Yi, Y., Qin, Y., Wang, L., Liu, G., Wu, Y., *et al.* (2016). Perchlorate degradation in aqueous solution using chitosan-stabilized zero-valent iron nanoparticles. *Separation and Purification Technology, 171*, 164–173.

Xie, Y., Dong, H., Zeng, G., Zhang, L., Cheng, Y., Hou, K., *et al.* (2017). The comparison of Se(IV) and Se(VI) sequestration by nanoscale zero-valent iron in aqueous solutions: The roles of solution chemistry. *Journal of Hazardous Materials, 338*, 306–312.

Xiong, K., Gao, Y., Zhou, L., & Zhang, X. (2016). Zero-valent iron particles embedded on mesoporous silica–carbon for chromium (VI) removal from aqueous solution. *Journal of Nanoparticle Research, 18*, 267.

Xu, P., Zeng, G. M., Huang, D. L., Feng, C. L., Hu, S., Zhao, M. H., *et al.* (2012). Use of iron oxide nanomaterials in wastewater treatment: A review. *Science of the Total Environment, 424*, 1–10.

Xue, W., Huang, D., Zeng, G., Wan, J., Zhang, C., Xu, R., *et al.* (2017). Nanoscale zero-valent iron coated with rhamnolipid as an effective stabilizer for immobilization of Cd and Pb in river sediments. *Journal of Hazardous Materials, 341*, 381–389.

Xie, Y., Dong, H., Zeng, G., Tang, L., & Jiang, Z. (2017). The interactions between nanoscale zero-valent iron and microbes in the subsurface environment: A review. *Journal of Hazardous Materials, 321*, 390–407.

Yan, W., Lien, H.-L., Koel, B. E., & Zhang, W. (2013). Iron nanoparticles for environmental clean-up: Recent developments and future outlook. *Environmental Science: Processes & Impacts, 15*, 88–98.

Yin, W., Wu, J., Li, P., Wang, X., Zhu, N., Wu, P., & Yang, B. (2012). Experimental study of zero-valent iron induced nitrobenzene reduction in groundwater: The effects of pH, iron dosage, oxygen, and common dissolved anions. *Chemical Engineering Journal, 184*, 198–204.

Yirsaw, B. D., Megharaj, M., Chen, Z., & Naidu, R. (2015). Environmental application and ecological significance of nano-zero valent iron. *Journal of Environmental Sciences, 44*, 88–98.

Z, L., L, W., J, M., X, L., J, X., F, W., *et al.* (2017). Zeolite-supported nanoscale zero-valent iron: New findings on simultaneous adsorption of Cd(II), Pb(II), and As(III) in aqueous solution and soil. *Journal of Hazardous Materials, 344*, 1–11.

Zeng, G., Chen, M., & Zeng, Z. (2013). Risks of neonicotinoid pesticides. *Science, 340*, 1403.

Zeng, Y., Walker, H., & Zhu, Q. (2017). Reduction of nitrate by NaY zeolite supported Fe, Cu/Fe and Mn/Fe nanoparticles. *Journal of Hazardous Materials, 324*, 605–613.

Zhou, X., Lv, B., Zhou, Z., Li, W., & Jing, G. (2015). Evaluation of highly active nanoscale zero-valent iron coupled with ultrasound for chromium(VI) removal. *Chemical Engineering Journal, 281*, 155–163.

Zhou, Y., Tang, L., Yang, G., Zeng, G., Deng, Y., Huang, B., *et al.* (2016). Phosphorus-doped ordered mesoporous carbons embedded with Pd/Fe bimetal nanoparticles for the dechlorination of 2,4-dichlorophenol. *Catalysis Science & Technology, 6*, 1930–1939.

Zhou, J., Sun, Q., Chen, D., Wang, H., & Yang, K. (2017). *Ochrobactrum anthropi* used to control ammonium for nitrate removal by starch-stabilized nanoscale zero valent iron. *Water Science and Technology, 76*, 1827–1834.

Zhu, B. W., Lim, T. T., & Feng, J. (2006). Reductive dechlorination of 1,2,4-trichlorobenzene with palladized nanoscale Fe⁰ particles supported on chitosan and silica. *Chemosphere, 65*, 1137–1145.

Zhu, F., Li, L., Ma, S., & Shang, Z. (2016). Effect factors, kinetics and thermodynamics of remediation in chromium contaminated soils by nanoscale zero valent Fe/Cu bimetallic particles. *Chemical Engineering Journal, 302*, 663–669.

Zeng, S., Duan, S., Tang, R., Li, L., Liu, C., & Sun, D. (2014). Adsorbent for dye removal: Synthesis and study on the kinetic and thermodynamic behaviors for dye adsorption. *Chemical Engineering Journal, 258*, 218–228.

Zhang, Z., Hu, S., Baig, S. A., Tang, J., & Xu, X. (2012). Catalytic dechlorination of Aroclor 1242 by Ni/Fe bimetallic nanoparticles. *Journal of Colloid and Interface Science, 385*, 160–165.

Zhang, Y., Wu, B., Xu, H., Liu, H., Wang, M., He, Y., & Pan, B. (2016). Nanomaterials-enabled water and wastewater treatment. *NanoImpact, 3–4*, 22–39.

Zhu, B. W., Lim, T. T., & Feng, J. (2006). Reductive dechlorination of 1,2,4-trichlorobenzene with palladized nanoscale Fe⁰ particles supported on chitosan and silica. *Chemosphere, 65*, 1137–1145.

IEER
Institute of Excellence in Education & Research